ACS OMEGA

Open Access

http://pubs.acs.org/journal/acsodf

Article

Chemical Constituents of *Aerides odorata* and Their Anti-Neuroinflammatory Effects on LPS-Activated BV2Microglial Cells

May Thazin Thant, Virunh Kongkatitham, Hnin Ei Ei Khine, Warisara Parichatikanond, Sanith Sri Jayashan, Preeyaporn Poldorn, Yutthana Wongnongwa, Pasarapa Towiwat, Chotima Böttcher, and Boonchoo Sritularak*

Cite This: https://doi.org/10.1021/acsomega.6c01737

Read Online

ACCESS | Metrics & More | Article Recommendations | Supporting Information

ABSTRACT: Comprehensive phytochemical study of the whole plants of *Aerides odorata* yielded 21 compounds, including two new phenanthrene derivatives (**1**−**2**), one new inseparable enantiomeric aurone glycoside (**3**) and 18 known compounds (**4**−**21**). The structures of the new compounds were elucidated by extensive spectroscopic analyses, encompassing NMR, MS, ultraviolet (UV), Fourier transform infrared spectroscopy (FT-IR), optical rotation, and CD data. The anti-inflammatory properties of some isolated compounds were evaluated in lipopolysaccharide activated BV2microglial cells. Among them, gigantol (**5**), nudol (**6**), coelonin (**9**), dihydrocorniferyl dihydro-*p*-coumarate (**10**), aerifalcatin (**14**), and 5-methoxy-9,10-dihydroxyphenanthrene-2,3,7-triol (**20**) exhibited potent inhibitory activity against nitric oxide production, with IC_{50} values of 1.82 ± 0.34, 4.88 ± 0.24, 2.42 ± 0.11, 4.67 ± 0.49, 1.37 ± 0.15, and 0.83 ± 0.15 μM, respectively. Furthermore, compounds **6**, **10**, and **20** significantly attenuated the release of proinflammatory cytokines TNF-α and IL-6 in a concentration-dependent manner. Notably, compound **20** appears to selectively modulate microglia-mediated neuroinflammation via regulation of NF-κB-dependent signaling pathways, leading to decreased production of key pro-inflammatory cytokines.

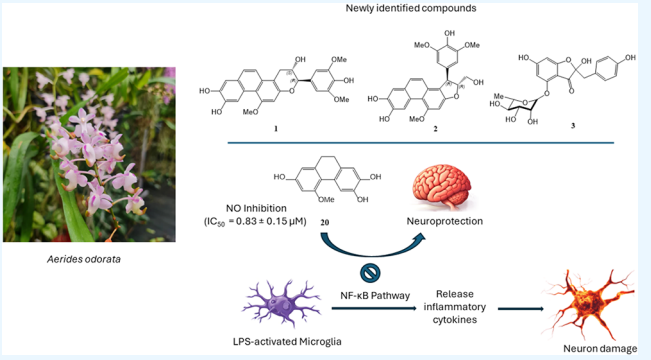

INTRODUCTION

A complex immune process that impacts the central nervous system (CNS), neuroinflammation is significant in the development and progression of several neurodegenerative illnesses, such as multiple sclerosis, Parkinson's disease, and Alzheimer's disease.[1] One key characteristic of neuroinflammation is the activation of microglia, which are the immune cells that reside in the brain. These cells change from a resting to an activated phenotype when they are stimulated by pathological insults, including tissue damage, β-amyloid accumulation, or lipopolysaccharide (LPS).[2] Activated microglia release a range of pro-inflammatory mediators, including nitric oxide (NO), prostaglandins, and cytokines, which can contribute to neuronal injury.[3] NF-κB-dependent signaling is a central molecular pathway that regulates inflammatory and immune responses by controlling the transcription of pro-inflammatory cytokines and mediators, and its dysregulation eventually contributes to chronic inflammation and neurodegenerative diseases.[4] Current therapeutic strategies for neuroinflammation mainly involve nonsteroidal anti-inflammatory drugs, corticosteroids, and immunomodulatory agents; however, their long-term use is often associated with limited efficacy and undesirable side effects. Several plant-derived compounds, including curcumin, resveratrol, and quercetin, have demonstrated neuroprotective and antineuroinflammatory activities through the modulation of oxidative stress, microglial activation, and inflammatory signaling pathway such as NF-κB.[5] In addition, numerous phenolic compounds and alkaloids isolated from medicinal plants have been reported to suppress nitric oxide and pro-inflammatory cytokine production in activated microglial cells.[6] These findings highlight the continued importance of natural product research for the discovery of novel agents targeting neuroinflammation-associated CNS diseases.

Aerides odorata Lour., a plant native to subtropical and tropical regions, belongs to the Orchidaceae family[7] and is known as "Ueang kulap krapaopit" in Thai.[8] The plant is ethnobotanically used to treat a variety of illnesses, including skin conditions, tuberculosis, cuts and wounds, pneumonia, inflammations, and chest and stomach discomfort.[9] In addition, the bactericidal properties of *A. odorata* have long

Received: February 13, 2026
Revised: June 23, 2026
Accepted: June 30, 2026

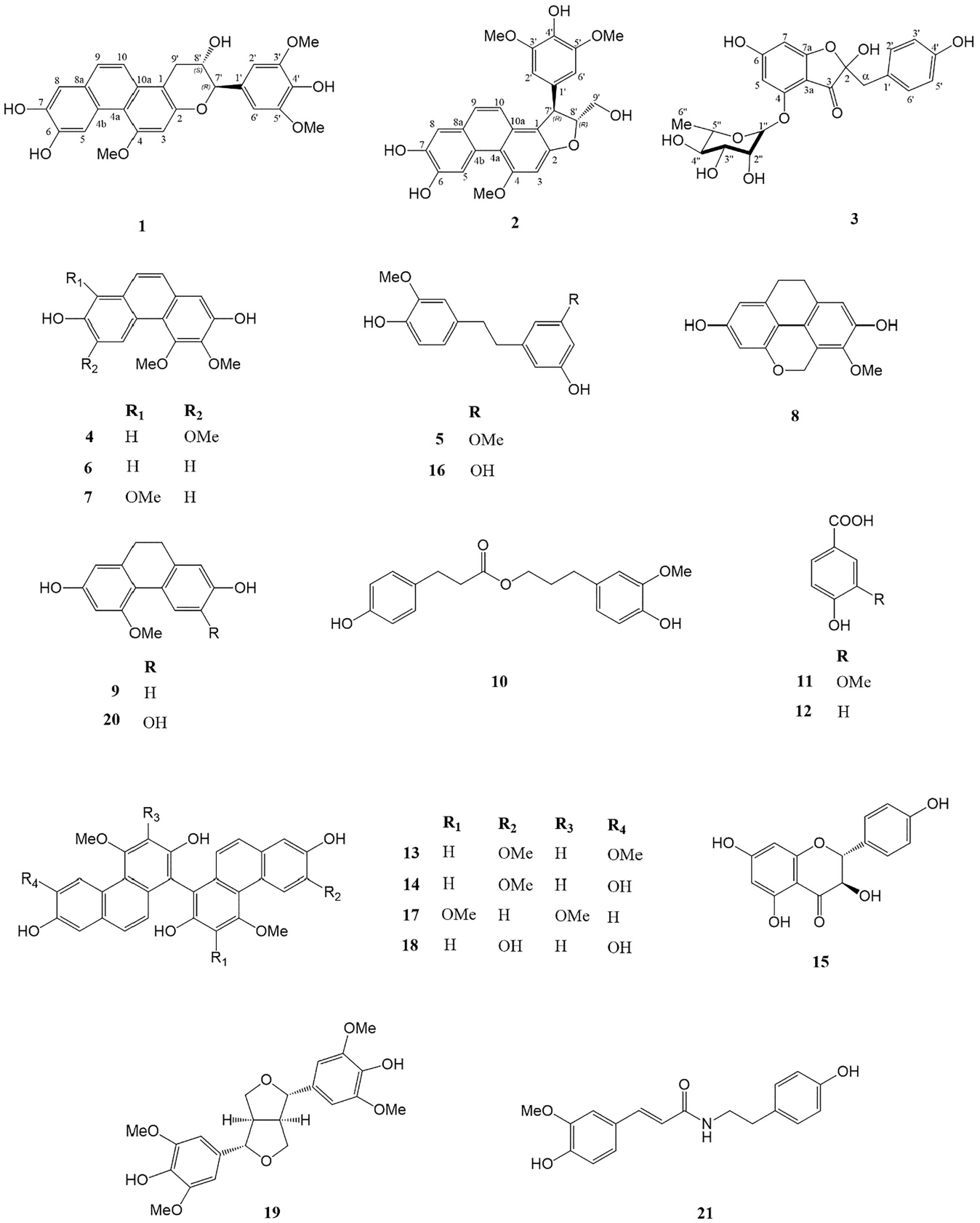

Figure 1. Chemical structures of compounds **1**−**21** isolated from *A. odorata*.

been recognized.[10] Previous studies have reported the presence of alkaloids, glycosides, flavonoids, saponins, tannins, terpenoids, steroids, and anthraquinones in *A. odorata*.[11] Studies conducted *in vitro* and *in vivo* have demonstrated the antioxidant potential and concentration-dependent hepatoprotective action of *A. odorata* extracts.[5] Furthermore, the ethyl

https://doi.org/10.1021/acsomega.6c01737
ACS Omega XXXX, XXX, XXX−XXX

acetate and methanolic extracts of *A. odorata* leaves have been reported for anticancer activity against two cancer cell lines (MCF-7 and HeLa).[9] However, no detailed phytochemical investigation of this plant has previously been reported. Our ongoing studies[12,13] focus on bioactive compounds derived from orchids. In this study, we explored the chemical constituents of *A. odorata* and evaluated their efficacy in alleviating neuroinflammation. Our preliminary findings showed that the ethyl acetate (EtOAc) extract (100 μg/mL) suppressed nitric oxide production by more than 80% in LPS-stimulated BV2microglial cells, prompting further investigation to identify the active constituents responsible for this effect. This study therefore provides the first detailed phytochemical investigation of *A. odorata* together with the evaluation of its antineuroinflammatory constituents.

RESULTS AND DISCUSSION

Structural Determination

Phytochemical investigation of *A. odorata* (EtOAc) extract revealed the presence of two new compounds, namely, aeriodins A and B (**1**–**2**), one inseparable enantiomeric aurone glycoside maesopsin-4-*O*-α-L-rhamnoside (**3**) and 18 known compounds, namely, 2,7-dihydroxy-3,4,6-trimethoxy-phenanthrene (**4**),[14] gigantol (**5**),[15] nudol (**6**),[16] confusarin (**7**),[17] imbricatin (**8**),[18] coelonin (**9**),[19] dihydrocorniferyl dihydro-*p*-coumarate (**10**),[20] vanillic acid (**11**),[21] *p*-hydroxy benzoic acid (**12**),[22] agrostonin (**13**),[23] aerifalcatin (**14**),[24] dihydrokaempferol (**15**),[25] tristin (**16**),[26] rigidanthrin (**17**),[27] aerimultin C (**18**),[28] syringaresinol (**19**),[29] 5-methoxy-9,10-dihydroxyphenanthrene-2,3,7-triol (**20**)[30] and *N-trans*-feruloyl tyramine (**21**)[31] (Figure 1).

Compound **1** was isolated as a brown amorphous solid. Its molecular formula was determined to be $C_{26}H_{24}O_8$ based on HR-ESIMS at *m*/*z* 463.1393 $[M-H]^-$ (calculated for $C_{26}H_{23}O_8$ at 463.1393) which revealed 15 degrees of unsaturation (Figure S1). The UV spectrum showed λ_{max} at 205, 265, 350, and 370 nm (Figure S2). FT-IR spectrum showed absorption peaks at 3288 cm^{-1} (hydroxy groups) and 1518, 1426 cm^{-1} (aromatic rings)[32] (Figure S3). The ^{1}H NMR spectrum of compound **1** displayed singlet aromatic proton signals at 6.76 (1H, s, H-3), 9.18 (1H, s, H-5) and 7.31 (1H, s, H-8), along with a pair of *ortho*-coupled methine protons at δ_H 7.68 (d, *J* = 8.8 Hz, H-9) and 7.63 (d, *J* = 8.8 Hz, H-10), indicating the presence of a phenanthrene skeleton.[33] The phenanthrene framework was supported by HMBC correlations of H-3 with C-1 (δ_C 106.7) and C-4a (δ_C 115.7), together with correlations from H-8 to C-4b (δ_C 125.3), C-6 (δ_C 145.5), and C-9 (δ_C 127.6).The methoxy signal at δ_H 4.09 displayed an HMBC correlation with C-4 (δ_C 157.9), whereas NOESY interactions with H-3 and H-5 further supported its assignment. The deshielded carbon signal at C-2 (δ_C 152.1) suggested an oxygen substitution at this site. Furthermore, the ^{1}H NMR spectrum revealed a phenylpropane moiety, as evidenced by the symmetrical singlet aromatic proton signals at δ_H 6.84 (2H, s, H-2′, H-6′), two equivalent methoxy proton signals at δ_H 3.86 (6H, s, MeO-3′,5′), two oxymethine proton signals at δ_H 4.72 (1H, d, *J* = 8.4 Hz, H-7′) and 4.30 (1H, m, H-8′), and methylene proton signals at δ_H 3.40 (1H, dd, *J* = 16.0, 6.0 Hz, H-9′a) and 3.02 (1H, dd, *J* = 16.0, 8.8 Hz, H-9′b). (Table 1). H-2′ and H-6′ exhibited HMBC correlations with C-7′ (δ_C 82.6). In addition, H-7′ showed HMBC correlations to C-2′/C-6′ (δ_C 105.4) and C-9′ (δ_C 31.6), while the COSY spectrum

Table 1. ^{1}H and ^{13}C-NMR Spectral Data of Compounds 1 and 2 in Acetone-d_6

	1[a]		2[b]	
position	^{1}H	^{13}C	^{1}H	^{13}C
1	-	106.7	-	115.6
2	-	152.1	-	158.9
3	6.76 (s)	98.7	6.80 (s)	93.9
4	-	157.9	-	160.9
4a	-	115.7	-	116.1
4b	-	125.3	-	126.6
5	9.18 (s)	112.8	9.09 (s)	113.5
6	-	145.5	-	145.0
7	-	144.4	-	146.4
8	7.31 (s)	111.6	7.17 (s)	111.6
8a	-	126.9	-	127.5
9	7.68 (d, 8.8)	127.6	7.37 (d, 8.8)	127.8
10	7.63 (d, 8.8)	118.8	7.10 (d, 8.8)	121.1
10a	-	132.5	-	131.3
1′	-	129.5	-	135.7
2′,6′	6.84 (s)	105.4	6.52 (s)	106.2
3′,5′	-	147.7	-	149.1
4′	-	135.9	-	135.9
7′	4.72 (d, 8.4)	82.6	4.75 (d, 5.8)	51.0
8′	4.30 (m)	67.8	4.66 (m)	94.4
9′	3.40 (dd, 16.0, 6.0) 3.02 (dd, 16.0, 8.8)	31.6	3.84 (m)	64.3
MeO-4	4.09 (s)	55.1	4.12 (s)	56.2
MeO-3′,5′	3.86 (s)	55.8	3.69 (s)	56.7
HO-4′	7.27 (s)	-	7.07 (s)	-
HO-6	-	-	8.32 (s)	-
HO-7	-	-	8.17 (s)	-

[a]^{1}H (400 MHz) and ^{13}C NMR (100 MHz); [b]^{1}H (600 MHz) and ^{13}C NMR (150 MHz)

revealed correlations of H-8′ with both H-7′ and H-9′. Furthermore, NOESY correlations were observed between MeO-3′ and H-2′, as well as between MeO-5′ and H-6′. HMBC correlations of H-9′ and H-7′ with C-2 (δ_C 152.1), revealed that the phenylpropane unit is attached to the phenanthrene framework at C-1 and C-2 through an ether linkage, thereby forming a dihydropyran ring. Moreover, the HMBC correlation between C-10a (δ_C 132.5) and H-9′ was also observed (Figure 2). The coupling constant (*J* = 8.4 Hz) between H-7′ and H-8′ suggested a *trans*-configuration between these two protons.[34] Structurally, compound **1** is closely related to the flavan-3-ol derivative (+)-fisetinidol, sharing a *trans*-configured arylpropanol unit, although in compound **1** this moiety is incorporated into a fused phenanthropyran framework. The CD spectrum of compound **1** showed positive Cotton effects at 233 and 292.7 nm and a negative Cotton effect at 260 nm (Figure S4). Previous studies have shown that (+)-fisetinidol displays a positive Cotton effect near 290 nm, whereas (−)-robinetinidol exhibits a negative Cotton effect in the same region. Therefore, the observed CD behavior of compound **1** is consistent with that of (+)-fisetinidol, supporting the proposed assignment of the 7′*R*,8′*S* configuration.[35] From these data, the structure of **1** was identified as (7′*R*, 8′*S*)-6,7,8′-trihydroxy-4-methoxy-7′-(4′-hydroxy-3′,5′-dimethoxyphenyl)-phenanthropyran and given the trival name aeriodin A.

Compound **2** was isolated as a brown amorphous solid. Its molecular formula was determined to be $C_{26}H_{24}O_8$ based on

https://doi.org/10.1021/acsomega.6c01737
ACS Omega XXXX, XXX, XXX−XXX

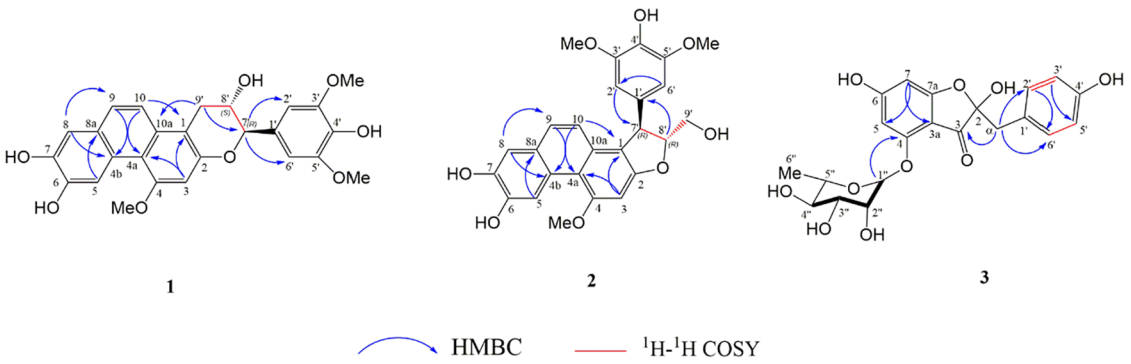

Figure 2. Key HMBC and ^{1}H−^{1}H COSY correlations of compounds **1**−**3**.

HR-ESIMS at *m*/*z* 463.1388 [M-H]$^-$ (calculated for $C_{26}H_{23}O_8$ at 463.1393) which revealed 15 degrees of unsaturation (Figure S13). The UV spectrum showed λ_{max} at 230, 265, 355, and 375 nm (Figure S14). FT-IR spectrum showed absorption peaks at 3365, 2924, 1589, and 1461 cm^{-1} which were characteristic to hydroxyl and aromatic moieties[32] (Figure S15). The ^{1}H NMR spectrum of compound **2** (Table 1) displayed resonances for five aromatic protons at δ_H 6.80 (1H, s, H-3), 9.09 (1H, s, H-5), 7.17 (1H, s, H-8), and *ortho*-coupled methine protons at δ_H 7.37 (d, *J* = 8.8 Hz, H-9) and 7.10 (d, *J* = 8.8 Hz, H-10), suggesting the presence of a phenanthrene core similar to that of compound **1**. The methoxy signal at δ_H 4.12 (3H, s, MeO-4) exhibited NOESY correlations with H-3 and H-5 of the phenanthrene unit. The ^{1}H NMR spectrum also indicated the presence of a phenylpropane moiety, as shown by two equivalent singlet aromatic proton signals at δ_H 6.52 (2H, s, H-2′, H-6′), a symmetry of two methoxy groups at δ_H 3.69 (6H, s, MeO-3′, MeO-5′), a methine at δ_H 4.75 (1H, d, *J* = 5.8 Hz, H-7′), an oxymethine proton at δ_H 4.66 (1H, m, H-8′), and an oxygenated methylene at δ_H 3.84 (2H, m, H-9′). The HMBC correlations of H-7′ with C-2′, C-6′ (δ_C 106.2), and C-9′ (δ_C 64.3), NOESY interactions between H-7′ and H-2′/H-6′, as well as between H-2′/H-6′ and H-8′, and COSY correlations connecting H-8′ with H-7′ and H-9′. NOESY cross-peaks were observed between MeO-3′ protons and H-2′, and between MeO-5′ protons and H-6′. The phenylpropane unit was linked to the phenanthrene core at C-1 (δ_C 115.6) and C-2 (δ_C 158.9) via an ether linkage, as evidenced by the HMBC correlation from H-7′ to C-2, indicating the presence of a dihydrofuran ring (Figure 2).[36] NOESY spectrum was used to demonstrate the relative stereo configuration of compound **2**, showing cross peaks between H-8′ and H-2′/6′, indicating that both protons reside on the same side. Furthermore, the 5.8 Hz coupling constant between H-7′ and H-8′ agreed with the values published in the literature for the relative *trans*-configuration.[37] The experimental electronic circular dichroism (ECD) spectrum of compound **2** displayed a negative Cotton effect at 209 nm and a positive Cotton effect at 228.9 nm. These spectral characteristics aligned with the *RR*-**2** curve in the calculated ECD (Figure 3), indicating that the absolute configurations of C-7′ and C-8′ in compound **2** were proposed to be *RR*. Therefore, compound **2** was identified as (7′*R*,8′*R*)-7′-(4′-hydroxy-3′,5′-dimethoxyphenyl)-8′-(hydroxymethyl)-4-methoxy-7′,8′-dihydrophenanthro[2,1-*b*]furan-6,7-diol and named aeriodin B.

Compound **3** was isolated as a whitish-brown amorphous solid. Its molecular formula was determined to be $C_{21}H_{22}O_{10}$

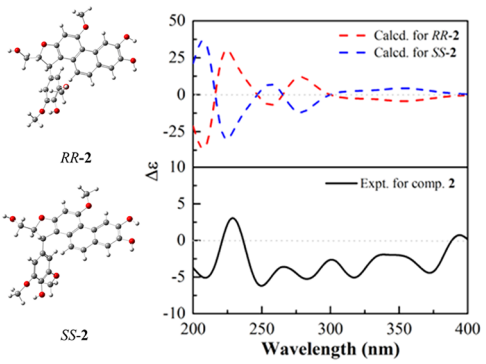

Figure 3. Calculated and experimental ECD spectra of **2**.

based on HR-ESIMS at *m*/*z* 433.1129 [M-H]$^-$ (calculated for $C_{21}H_{21}O_{10}$ at 433.1134) which revealed 11 degrees of unsaturation (Figure S27). The UV spectrum showed λ_{max} at 205, 230, and 285 nm (Figure S28). FT-IR spectrum showed absorption peaks at 3275, 2934, 1599, and 1445 cm^{-1} which were characteristic to hydroxyl and aromatic moieties (Figure S29).[32] The ^{1}H and ^{13}C NMR spectra (Table 2) of compound **3** displayed two sets of signals. Each pair of signals had an intensity ratio of 1:1. Two doublet pairs for H-5 at δ_H 6.12 (1H, d, *J* = 1.6 Hz), 6.07 (1H, d, *J* = 1.6 Hz), and two doublet pairs for H-7 at δ_H 5.94 (1H, d, *J* = 1.6 Hz), 5.91 (1H, d, *J* = 1.6 Hz), were observed in its ^{1}H NMR spectra, which integrated for *meta*-coupled protons. Two further doublet pairs of H-2′,6′ at δ_H 6.90 (2H, d, *J* = 8.4 Hz), 7.01 (2H, d, *J* = 8.4 Hz), and H-3′,5′ at δ_H 6.59 (2H, d, *J* = 8.4 Hz), 6.57 (2H, d, *J* = 8.4 Hz) are integrating into *ortho*-coupled protons. There are two doublet signals at δ_H 3.06 (2H, d, *J* = 14.1 Hz) and 3.10 (2H, d, *J* = 14.4 Hz) that are attributed to the methylene (H_2-α) on the aromatic ring. The ^{13}C NMR spectrum displayed distinctive resonances attributable to the ketonic carbons of aurone derivatives at δ_C 194.6 and 194.5 along with the typical signals for aromatic carbons.[38] Additionally, the ^{1}H and ^{13}C NMR spectra of compound **3** showed good agreement with maesopsin, an aurone derivative, isolated from the barks of *Hovenia trichocarea*, indicating that the aglycone part of **3** was maesopsin.[39] Maesopsin's reversible hemiketal at C-2 allows it to exist in enantiomeric pairs. Upon glycosylation, maesopsin forms two diastereoisomers, which results in the formation of two sets of signals.[40] In addition, the observation of two clearly separated sets of signals with an approximately 1:1 ratio in both the ^{1}H and ^{13}C NMR spectra is more consistent with the presence of inseparable stereoisomeric forms than with conformational effects, which usually produce broadened or

https://doi.org/10.1021/acsomega.6c01737
ACS Omega XXXX, XXX, XXX−XXX

Table 2. ^{1}H (400 MHz) and ^{13}C NMR (100 MHz) Spectral Data of Compound 3 in Methanol-d_4

position	^{1}H	^{13}C
2	-	106.2, 106.0
3	-	194.6, 194.5
3a	-	102.9, 102.7
4	-	155.8, 155.5
5	6.12 (1H, d, 1.6)	96.2, 95.9
	6.07 (1H, d, 1.6)	
6	-	169.4, 169.3
7	5.94 (1H, d, 1.6)	91.7, 91.6
	5.91 (1H, d, 1.6)	
7a	-	173.0, 172.9
α	3.10 (2H, d, 14.4)	40.9, 40.6
	3.06 (2H, d, 14.1)	
1′	-	124.4, 124.2
2′, 6′	7.01 (2H, d, 8.4)	131.2, 131.1
	6.90 (2H, d, 8.4)	
4′	-	155.8, 155.8
3′, 5′	6.59 (2H, d, 8.4)	114.4, 114.3
	6.57 (2H, d, 8.4)	
1″	5.48 (1H, d, 1.6)	98.4, 98.0
	5.45 (1H, d, 1.6)	
2″	4.07 (2H, m)	70.2, 70.1
3″	3.96 (2H, m)	70.6, 70.6
4″	3.46 (2H, m)	72.2, 72.2
5″	3.57 (2H, m)	69.8, 69.7
6″	1.22 (3H, d, 6.0)	16.7, 16.6
	1.19 (3H, d, 6.0)	

variable NMR signals. The glycone moiety is suggested to be rhamnose sugar by a doublet pair for H-6″ at δ_H 1.19 (3H, d, J = 6.0 Hz) and 1.22 (3H, d, J = 6.0 Hz). One pair of anomeric proton signals appeared at δ_H 5.48 (1H, d, J = 1.6 Hz) and 5.45 (1H, d, J = 1.6 Hz), indicated the rhamnose to have a α-configuration.[41] While acid hydrolysis and comparison with authentic sugar standards would offer more definitive evidence for the sugar absolute configuration, such experiments could not be performed because compound **3** was isolated in small amounts. The HMBC experiment established the location of sugar connections to the aglycone. Connectivity between H-1″ of rhamnose and C-4 (δ_C 155.8/155.5) of the aglycone suggested the presence of a rhamnosyl unit at C-4 (Figure 2). Compound **3** was determined as the inseparable enantiomeric aurone glycoside, maesopsin-4-*O*-α-L-rhamnoside, based on the spectrum data above.

Cytotoxicity Evaluation of Isolated Compounds in BV2Microglial Cells

Isolated compounds from *A. odorata* were evaluated for cytotoxicity in BV2microglial cells across a range of concentrations (0−40 μM). Due to limited quantities, compounds **8**, **11**, **12**, **15**, **16**, and **17** were not included in the assessment (Table 3). The highest concentration that did not significantly reduce cell viability compared with the untreated control group was considered the safe concentration. Based on this criterion, concentrations below 5 μM were considered relatively safe for most tested compounds. However, compound **2** reduced cell viability to 77.10 ± 8.04% at 5 μM, while compound **13** showed marked cytotoxicity at the same concentration.

Inhibition of Nitric Oxide Release by Tested Compounds in Activated Microglial Cells

Excessive NO production is a hallmark of neuroinflammation linked to CNS disorders.[42] Although NO serves important physiological functions, such as supporting normal neuronal activity and synaptic plasticity, its abnormal accumulation can be harmful. Upon stimulation by inflammatory signals such as LPS or cytokines, microglia upregulate inducible nitric oxide synthase (iNOS), leading to excessive NO production. Overproduction of NO contributes to cellular stress, mitochondrial dysfunction, and neuronal injury, all of which are commonly observed in neurodegenerative diseases.[43] Therefore, strategies aimed at limiting NO release have gained attention to protect neurons and potentially slow the onset and progression of CNS-related conditions.

Table 3. Evaluation of Cytotoxicity Profiles of *A. odorata* Compounds in BV2Microglial Cells[a]

	cell viability (%) (mean ± SD)				
compound	0 μM	5 μM	10 μM	20 μM	40 μM
1	100 ± 0	99.10 ± 4.78	92.86 ± 0.78	88.72 ± 4.77*	60.63 ± 3.76***
2	100 ± 0	77.10 ± 8.04**	72.49 ± 4.73**	67.30 ± 6.49***	61.18 ± 2.38***
3	100 ± 0	105.42 ± 5.10	100.59 ± 2.58	73.86 ± 10.50**	43.54 ± 1.37***
4	100 ± 0	105.66 ± 4.16	102.68 ± 2.38	88.02 ± 5.05**	44.14 ± 2.38***
5	100 ± 0	95.64 ± 0.57	94.8 ± 1.23	91.31 ± 0.51	74.75 ± 1.61**
6	100 ± 0	95.72 ± 2.15	92.06 ± 0.5	55.41 ± 11.23***	18.20 ± 5.41***
7	100 ± 0	107.72 ± 0.76	100.51 ± 0.32	90.47 ± 2.97*	57.35 ± 3.14***
9	100 ± 0	105.13 ± 3.95	97.30 ± 5.34	73.04 ± 4.01**	28.25 ± 6.83***
10	100 ± 0	100.51 ± 2.92	96.35 ± 0.91	90.45 ± 4.05*	86.82 ± 5.09**
13	100 ± 0	31.42 ± 6.06***	22.13 ± 2.00***	15.92 ± 1.32***	10.95 ± 2.37***
14	100 ± 0	103.73 ± 4.28	49.98 ± 3.96***	29.45 ± 1.88***	16.34 ± 1.88***
18	100 ± 0	99.16 ± 4.11	94.13 ± 2.59	19.26 ± 1.27***	12.92 ± 2.22***
19	100 ± 0	92.53 ± 6.16	91.51 ± 0.38	86.38 ± 2.25**	83.43 ± 2.38**
20	100 ± 0	102.68 ± 7.17	94.72 ± 2.02	35.84 ± 3.92***	12.05 ± 2.60 ***
21	100 ± 0	99.25 ± 1.15	97.00 ± 2.62	96.25 ± 3.27	93.03 ± 2.83

[a]Data are presented as mean ± SD (n = 3). Statistical differences between treatment groups and vehicle control were analyzed using one-way ANOVA followed by Dunnett's post hoc test. Statistically significant reductions in cell viability are indicated by *, ** and *** corresponding to p-values of <0.05, < 0.01 and <0.001 respectively. Cell viability values exceeding 100% reflect normalization to the untreated control and normal assay variability and do not indicate significant cell proliferation.

https://doi.org/10.1021/acsomega.6c01737
ACS Omega XXXX, XXX, XXX−XXX

In the present study, compounds **1**, **3**, **4**, **5**, **6**, 7, **9**, **10**, **14**, **18**, **19**, **20**, and **21** were evaluated for their ability to inhibit nitric oxide (NO) release at a nontoxic concentration of 5 μM. As shown in Table 4, gigantol (**5**), nudol (**6**), coelonin (**9**), dihydrocorniferyl dihydro-*p*-coumarate (**10**), aerifalcatin (**14**), and 5-methoxy-9,10-dihydroxyphenanthrene-2,3,7-triol (**20**) exhibited notable half maximal inhibitory concentration for nitric oxide production (IC_{50}) values of 1.82 ± 0.34, 4.88 ± 0.24, 2.42 ± 0.11, 4.67 ± 0.49, 1.37 ± 0.15, and 0.83 ± 0.15 μM, respectively. These results indicate that these compounds exert stronger NO-suppressive effects than the reference drug, minocycline (IC_{50} = 7.66 ± 0.31 μM).

Table 4. Nitric Oxide Inhibition (IC_{50}) of Isolated Compounds from *A. odorata* in LPS-Activated BV2Microglial Cells[a]

compound	IC_{50} (μM, mean ± SD)
1	>5
3	>5
4	>5
5	1.82 ± 0.34
6	4.88 ± 0.24
7	>5
9	2.42 ± 0.11
10	4.67 ± 0.49
14	1.37 ± 0.15
18	>5
19	>5
20	0.83 ± 0.15
21	>5
minocycline	7.66 ± 0.31

[a]Data are presented as mean ± SD (n = 3).

Notably, the new compounds **1** and **3** did not exhibit significant antineuroinflammatory activity in the present study. Structural comparison with the active compounds suggests that anti-inflammatory activity may be influenced by the number and accessibility of free phenolic hydroxyl groups, which contribute to modulation of inflammatory signaling pathways and oxidative stress responses. In compound **1**, the rigid phenanthropyran framework and methoxy substitution pattern may reduce the availability of active hydroxyl functionalities involved in cytokine suppression. Compound **2** was not further evaluated due to limited quantity and preliminary cytotoxicity at 5 μM in BV2 cells. In compound **3**, glycosylation of the aurone scaffold may reduce cellular uptake or interactions with intracellular inflammatory targets, leading to weaker activity. Further SAR studies, including evaluation of structurally related derivatives, are needed to clarify the structural features governing antineuroinflammatory activity.

Nevertheless, the related phenanthrene and aurone derivatives have been reported to exhibit antioxidant and antiviral activities,[44] suggesting that new compounds **1**−**3** may possess other biological properties requiring further investigation.

Modulation of TNF-α and IL-6 Expression by Selected Compounds in LPS-Induced Microglial Cells

Lipopolysaccharide-activated microglia produce TNF-α and IL-6, key mediators that promote neuroinflammation, neuronal

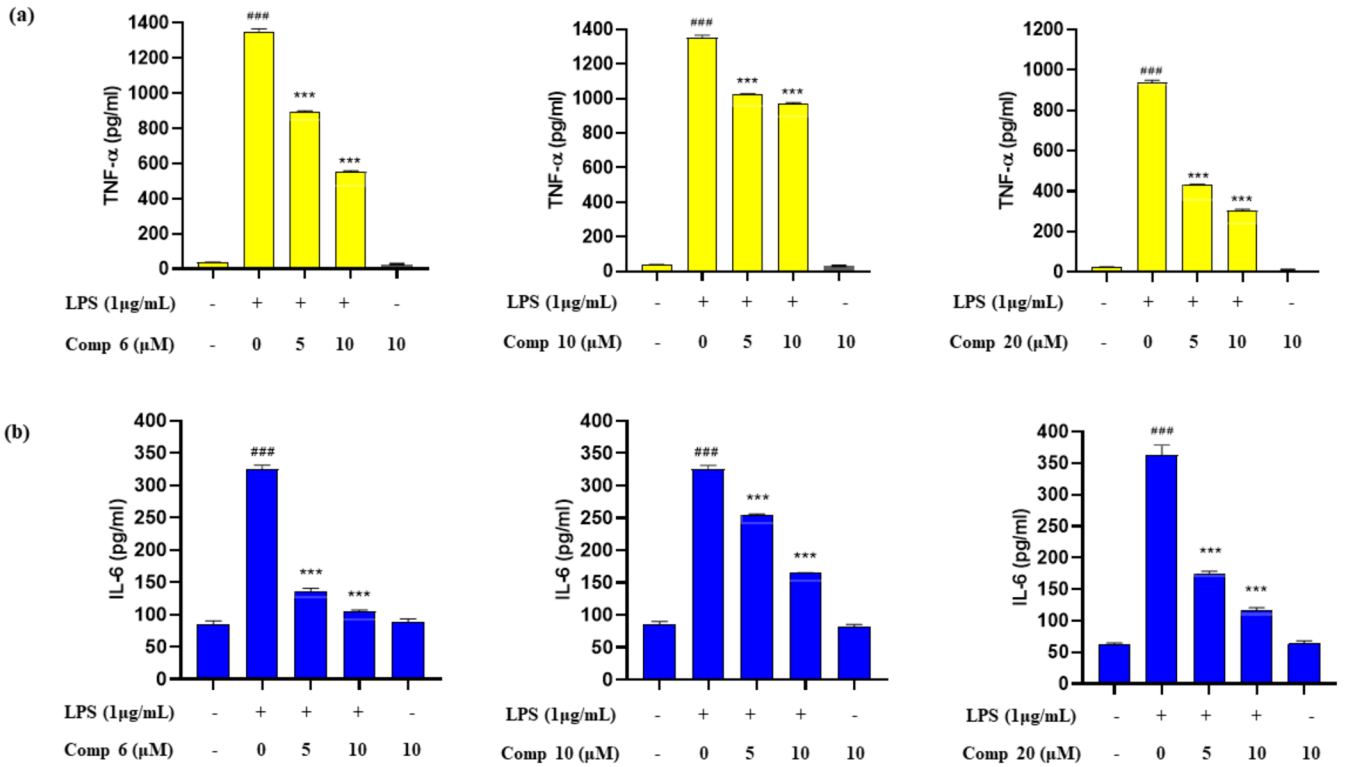

Figure 4. Effects of nudol (**6**), dihydrocorniferyl dihydro-*p*-coumarate (**10**), and 5-methoxy-9,10-dihydroxyphenanthrene-2,3,7-triol (**20**) on the release of TNF-α (a) and IL-6 (b) in LPS-induced BV2microglial cells. Following 1 h pretreatment with compounds **6**, **10** and **20** (5 μM and10 μM), cells were exposed to LPS (1 μg/mL) for 24 h, and cytokine levels were determined by ELISA. Values represent mean ± SD of three independent experiments. ### indicates a significant difference between the vehicle and LPS-treated group (p < 0.001), while *** indicates significant differences compared to the LPS-treated group at p < 0.001.

https://doi.org/10.1021/acsomega.6c01737
ACS Omega XXXX, XXX, XXX−XXX

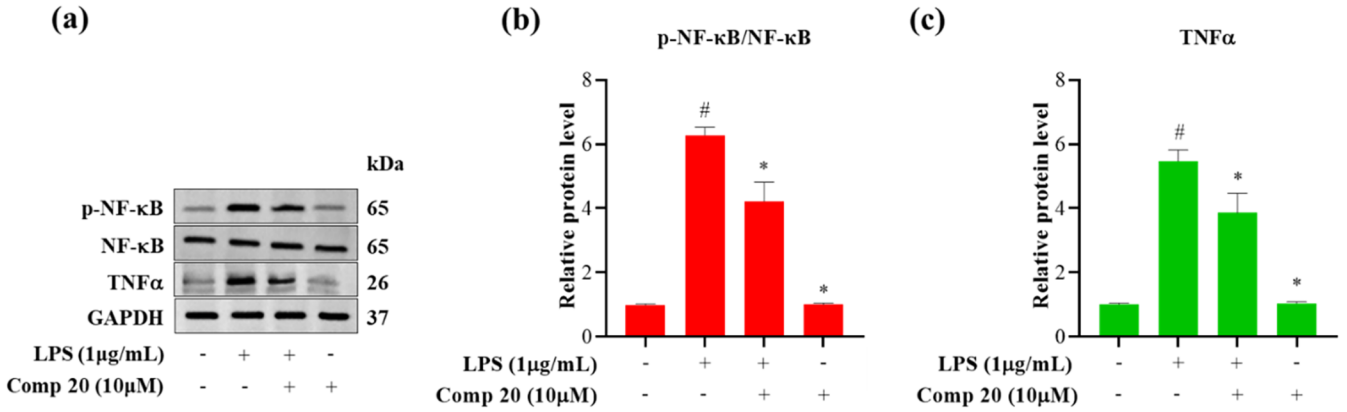

Figure 5. Effects of compound **20** on inflammatory signaling in LPS-stimulated BV2microglial cells. Protein expression levels were assessed by Western blotting. (a) Representative Western blot images of p-NF-κB, NF-κB, TNF-α and GAPDH. Quantitative analysis of (b) p-NF-κB/NF-κB and (c) TNF-α protein expression was performed, with GAPDH used as the loading control. Data are presented as mean ± SD from at least four independent experiments. $^{\#}p < 0.05$ denotes significant compared to control. $^{*}p < 0.05$, compared to LPS.

dysfunction, and neurodegeneration. Modulating these cytokines offers a potential therapeutic approach for managing neuroinflammatory diseases.[45] In the present study, the effects of compounds **6**, **10**, and **20** on the expression of TNF-α and IL-6 were evaluated in LPS-stimulated BV2microglial cells. Although compounds **5**, **9**, and **14** also demonstrated strong NO inhibitory activity, they were not re-evaluated in this assay due to previous reports confirming their TNF-α and IL-6 suppression.[24,45] As illustrated in Figure 4, LPS stimulation markedly increased the production of proinflammatory cytokines, whereas pretreatment with nudol (**6**), dihydrocorniferyl dihydro-*p*-coumarate (**10**), and 5-methoxy-9,10-dihydroxyphenanthrene-2,3,7-triol (**20**) significantly attenuated TNF-α and IL-6 secretion in a concentration-dependent manner. This study newly reveals the antineuroinflammatory effects of compounds **6**, **10**, and **20**, highlighting their ability to suppress the release of proinflammatory mediators in activated microglial cells.

Phenanthrene and dihydrophenanthrene derivatives have been widely reported to exhibit anti-inflammatory and antineuroinflammatory activities in LPS-activated microglial models. For example, phenanthrene derivatives from *Bletilla striata* showed significant suppression of pro-inflammatory mediators in BV2microglial cells.[46] In the present study, nudol (**6**) is consistent with previously reported phenanthrenes that modulate NF-κB and MAPK signaling pathways. Similarly, coelonin and related dihydrophenanthrene derivatives have been reported to suppress inflammatory responses in microglial and other cellular models, supporting the relevance of this scaffold in inflammation regulation.[47] Notably, compound **20**, a dihydrophenanthrene derivative, showed stronger inhibition of TNF-α and IL-6 than structurally similar compound, coelonin (**9**), suggesting that additional hydroxyl substitution in **20** may enhance activity via improved hydrogen bonding and target interactions. In addition, the result of dihydrocorniferyl dihydro-*p*-coumarate (**10**) is consistent with previous report demonstrating that other phenylpropanoid ester derivatives such as 4-methoxycinnamyl *p*-coumarate, inhibit NO and pro-inflammatory mediators via NF-κB, MAPK, and Nrf2/HO-1 pathways.[48] These results highlight the importance of phenanthrene and phenylpropanoid frameworks in regulating neuroinflammation.

Compound 20 Suppresses LPS-Induced NF-κB Activation and TNF-α Expression in BV2Microglial Cells

Compound **20** was selected for mechanistic investigation because of its potent inhibitory effect on nitric oxide production (IC_{50} = 0.83 ± 0.15 μM). To elucidate the effects of compound **20** on LPS-induced inflammatory signaling in BV2microglial cells, Western blot analysis was performed to determine changes in the protein expression of key inflammatory markers and their associated signaling pathways (Figure 5). LPS stimulation significantly increased the p-NF-κB/NF-κB ratio and TNF-α expression compared with the control group, indicating effective induction of inflammatory signaling and its main effector by LPS. Pretreatment with compound **20** markedly attenuated LPS-induced NF-κB activation and reduced TNF-α protein levels compared with LPS treatment alone. In contrast, treatment with compound **20** alone did not result in significant changes in the p-NF-κB/NF-κB ratio or TNF-α expression relative to control cells. These results indicate that compound **20** does not elicit inflammatory activation under basal conditions but effectively suppresses LPS-mediated inflammatory signaling. Collectively, these findings suggest that compound **20** may selectively regulate microglia-mediated neuroinflammation through modulation of NF-κB−dependent signaling pathways, leading to reduced production of the key pro-inflammatory cytokine, TNF-α.

CONCLUSION

In summary, the phytochemical investigation of the whole plants of *Aerides odorata* resulted in the isolation of 21 compounds, comprising three new compounds (**1**−**3**) and 18 known compounds (**4**−**21**). Among them, gigantol (**5**), nudol (**6**), coelonin (**9**), dihydrocorniferyl dihydro-*p*-coumarate (**10**), aerifalcatin (**14**), and 5-methoxy-9,10-dihydroxyphenanthrene-2,3,7-triol (**20**) exhibited notable nitric oxide inhibition activity with IC_{50} values ranging from 0.83 ± 0.15 to 4.88 ± 0.24 μM. Furthermore, nudol (**6**), dihydrocorniferyl dihydro-*p*-coumarate (**10**), and 5-methoxy-9,10-dihydroxyphenanthrene-2,3,7-triol (**20**) significantly reduced TNF-α and IL-6 secretion in LPS-stimulated BV2microglial cells in a concentration-dependent manner. This study newly reveals the antineuroinflammatory effects of compounds **6**, **10**, and **20**, highlighting compound **20** as a promising lead candidate for

https://doi.org/10.1021/acsomega.6c01737
ACS Omega XXXX, XXX, XXX−XXX

the development of novel therapeutics targeting microglia-mediated neuroinflammation.

MATERIALS AND METHODS

General Experimental Procedures

Instruments

Optical rotation was measured using a Jasco P-2000 digital polarimeter (Easton, MD). UV spectra were recorded on a Milton Roy Spectronic 3000 Array spectrophotometer (Rochester, Monroe, NY). CD spectra were obtained with a Jasco J-815 CD spectrophotometer (Hachioji, Tokyo, Japan). FT-IR spectra were acquired on a PerkinElmer FT-IR 1760X spectrophotometer (Boston, MA). Mass spectra were recorded using a Bruker MicroTOF mass spectrometer (ESI-MS) (Billerica, MA). NMR spectra were obtained on a Bruker Avance Neo 400 MHz NMR spectrometer (Billerica, MA) and a Bruker Avance III HD 600 NMR spectrometer (Billerica, MA).

Chromatographic Materials. Vacuum-liquid chromatography (VLC) and column chromatography (CC) were performed using silica gel 60 (No. 1.07734.2500) with a particle size of 0.063−0.200 mm and (No. 1.09385.2500) with a particle size of 0.040−0.063 mm (Merck, NJ). Gel filtration chromatography was carried out using Sephadex LH-20 (Merck, NJ). The initial assessment of the purity of isolated compounds was performed using thin-layer chromatography (TLC) on silica gel 60 F254 plates (Merck, NJ) under UV light.

Plant Material

A. odorata plants were purchased from Chatuchak market in November 2022. Plant identification was carried out by Mr. Yanyong Punpreuk, Department of Agriculture, Ministry of Agriculture and Cooperatives, Bangkok, Thailand. A voucher specimen (BS-AO-2565) has been deposited at the Department of Pharmacognosy and Pharmaceutical Botany, Faculty of Pharmaceutical Sciences, Chulalongkorn University.

Extraction and Isolation

The dried powder of whole plants of *A. odorata* (2 kg) was macerated with MeOH (4 × 6 L). Then, the methanolic extract (313.3 g) was dissolved in water and partitioned with ethyl acetate (EtOAc) to give an EtOAc extract (79.6 g) and an aqueous extract (230 g). The EtOAc extract was then separated by vacuum liquid chromatography (silica gel, using a gradient of hexane- EtOAc, 100:0 → 0:100, v/v) to give nine fractions (A-I).[36] Fraction B (3 g) was fractionated on a silica gel column (Acetone- hexane, 2.5:7.5) to give 3 fractions (BA-BC). Fraction BB (88.3 mg) was separated on a silica gel column using dichloromethane solvent to yield compounds **4** (5.1 mg), **5** (5.3 mg), **6** (2 mg) and **7** (2.6 mg). Fraction C (2 g) was subjected to CC (silica gel, dichloromethane- EtOAc, 100:0 → 0:100, v/v) and fractions (CA-CG) were obtained. Fraction CB (200 mg) was separated by Sephadex LH-20 (acetone) and then fractions (CB1 and CB2) were obtained. Fraction CB1 (10 mg) was subjected to PTLC (Methanol- dichloromethane, 0.2:9.8, 2 times) and then compound **8** (1.4 mg) and compound **9** (2.2 mg) were obtained. Fraction CC (800 mg) was separated by Sephadex LH-20 (acetone) to yield fractions CC1 and CC2. Fraction CC1 (20 mg) was separated again by Sephadex LH-20 (methanol) to produce compound **10** (10 mg). Fraction CF (100 mg) was separated again by Sephadex LH-20 (methanol) to yield compound **11** (1 mg). Fraction CG (200 mg) was subjected to CC (silica gel, EtOAc- hexane, 3.5:6.5) and then pure compound **12** (4 mg) was obtained. Fraction E (3.5 g) was fractionated on a silica gel column dichloromethane- EtOAc (100:0 → 0:100, v/v) to give 3 fractions (EA-EC). Fraction EA (1.2 g) was subjected to CC (silica gel, EtOAc- hexane, gradient) followed by Sephadex LH-20 (methanol) to yield compound **13** (3.5 mg). Fraction EB (1g) was separated by Sephadex LH-20 (acetone) and then fractions (EB1-EB3) were obtained. Fraction EB3 (500 mg) was subjected to CC (silica gel, dichloromethane- EtOAc, 100:0 → 0:100, v/v) and then Sephadex LH-20 (methanol) to give compound **14** (2 mg) and compound **15** (2 mg). Fraction EB1 (50 mg) was separated again by Sephadex LH-20 (methanol) to furnish compound **16** (1 mg) and EB1a (4 mg) which was further fractionated on a silica gel column (EtOAc- dichloromethane, 2:8) to give compound **17** (0.8 mg). Fraction F (4.9 g) was subjected to CC silica gel, dichloromethane- EtOAc (100:0 → 0:100, v/v) to produce fractions (FA-FF). Fraction FF (1 g) was separated again by Sephadex LH-20 (acetone) to yield compound **18** (4 mg). Fraction FD (100 mg) was subjected to CC (silica gel, Methanol- dichloromethane, 0.2:9.8) and compound **19** (5 mg) was obtained. Fraction FC (250 mg) was subjected to PTLC (Methanol- dichloromethane, 0.2:9.8) to yield compound **20** (5 mg). Fraction FE (1 g) was separated by Sephadex LH-20 (acetone) and then Sephadex LH-20 (methanol) to yield FE1-FE4 fractions. Fraction FE1 (10 mg) was subjected to CC (silica gel, EtOAc- hexane, 1:1) to produce compound **21** (4 mg). Fraction FE3 (50 mg) was subjected to CC (silica gel, EtOAc- hexane, 4:6) to produce a new compound **1** (1.4 mg). Fraction FE4 (2 mg) was subjected to capillary CC (silica gel, Methanol- dichloromethane, 0.2:9.8) to produce new compound **2** (1 mg). Fraction G (8 g) was subjected to CC (silica gel, dichloromethane- MeOH,100:0 → 90:10, v/v) to produce fractions (GA-GD). Fraction GD (1 g) was separated with Sephadex LH-20 (acetone) and then CC (silica gel, Methanol-dichloromethane, 1:9) to furnish mixture of new compound **3** (6 mg).

Aeriodin A (1). Brown amorphous solid; $[\alpha]_D^{20}$ + 2.2 (*c* 0.1, MeOH); UV (MeOH) λ_{max} (log ε) 205 (4.11), 265 (4.19), 350 (3.15), 370 (3.25); HR-ESI-MS: $[M\text{-}H]^-$ at *m/z* 463.1393 (calcd. for $C_{26}H_{23}O_8$ 463.1393); IR: ν_{max} at 3288, 1518, and 1426 cm^{-1}; ECD (MeOH): λ_{max} ($\Delta\varepsilon$) 233 (+0.21), 260 (−0.38) and 292.7 (+0.14) nm.

Aeriodin B (2). Brown amorphous solid; $[\alpha]_D^{20}$ - 2.1 (*c* 0.05, MeOH); UV (MeOH) λ_{max} (log ε) 230 (4.21), 265 (3.97), 355 (3.14), 375 (3.11); HR-ESI-MS: $[M\text{-}H]^-$ at *m/z* 463.1388 (calcd. for $C_{26}H_{23}O_8$ 463.1392); IR: ν_{max} at 3365, 2924, 1589, and 1461 cm^{-1}; ECD (MeOH): λ_{max} ($\Delta\varepsilon$) 209 (−0.72) and 228.9 (+3.04) nm.

Maesopsin-4-*O*-*α*-L-Rhamnoside (3). Brown amorphous solid; UV (MeOH) λ_{max} (log ε) 205 (4.20), 230 (3.98), 285 (4.03); HR-ESI-MS: $[M\text{-}H]^-$ at *m/z* 433.1129 (calcd. for $C_{21}H_{21}O_{10}$ 433.1134); IR: ν_{max} at 3275, 2934, 1599, and 1445 cm^{-1}.

HPLC Purity Analysis

Purity analysis was performed using an Agilent 1290 Infinity II system (Agilent Technologies) equipped with a HALO C18−5. The mobile phase consisted of MeOH: H_2O (40:60 and 25:75) containing 0.1% formic acid in both solvents. The flow rate was maintained at 0.3 mL/min, with the column temperature set at 30 °C. The injection volume was 1 μL, and UV detection was carried out at 265 nm.

Computational Detail

The Density Functional Theory (DFT) calculations were employed to optimize the various configurations of compound **2** at the B3LYP/6−31G(d,p) level. Subsequently, Electron Circular Dichroism (ECD) spectra were computed via time-dependent DFT (TD-DFT) at the B3LYP/6−311++G(d,p) level, incorporating solvation effects modeled via the Polarizable Continuum Model (PCM) with methanol as the solvent. All computational analyses were performed using the Gaussian16 software package.[49] Additionally, the ECD spectra were simulated by applying overlapping Gaussian functions, parametrized with a fitting parameter (σ = 0.25 eV) through the SpecDis1.64 program,[50] with the length gauge representation for enhance accuracy.

BV2 Cell Culture

BV2microglial cells (AcceGen Biotechnology, Fairfield, NJ) were maintained in DMEM (PAN Biotech, Aidenbach, Germany) supplemented with 10% fetal bovine serum (PAN Biotech, Aidenbach, Germany) and 1% penicillin−streptomycin (GIBCO, Carlsbad, CA). All experiments were conducted using cells at passages 14−17. Cultures were incubated at 37 °C in a humidified atmosphere containing 5% CO_2 and were subcultured once they reached 70−80% confluence.[24]

https://doi.org/10.1021/acsomega.6c01737
ACS Omega XXXX, XXX, XXX−XXX

Cell Viability Assay

The cell viability assay was conducted to identify the nontoxic concentrations of the test compounds. Briefly, BV2 cells were seeded in 96-well plates at a density of 1×10^4 cells per well and incubated for 24 h. The cytotoxicity of the tested compounds was evaluated by measuring cell viability using the 3-(4,5-dimethylthiazol-2-yl)-2,5-diphenyltetrazolium bromide (MTT) (Sigma-Aldrich, St. Louis, MO) assay. After treatment, MTT solution (500 $\mu g \cdot mL^{-1}$) was added to each well and incubated for 3 h. The resulting formazan crystals were dissolved in DMSO, and the absorbance was read at 570 nm using a microplate reader.[24]

$$\text{cell viability (\%)} = \text{absorbance of treated cells} / \text{absorbance of control cells} \times 100$$

Nitrite Assay

Nitric oxide production was quantified by measuring nitrite accumulation using the Griess reaction. Untreated cells were used as the negative control, while minocycline was used as the positive control. BV2microglial cells treated with LPS alone served as the inflammatory control group. In brief, BV2 cells were seeded in 48-well plates at a density of 7.5×10^4 cells per well and incubated for 24 h. Subsequently, the cells were treated with tested compounds for 2 h, followed by coincubation with LPS (BioLegend, San Diego, CA) for an additional 24 h. After treatment, 100 μL of culture supernatant was mixed with an equal volume of Griess reagent (Sigma-Aldrich, St. Louis, MO) at a 1:1 ratio and incubated for 15 min at room temperature. Absorbance was then measured at 540 nm using a microplate reader, and nitrite concentration was determined.[51]

$$\text{NO inhibition (\%)} = (A_{control} - A_{sample}/A_{control}) \times 100$$

$A_{control}$ = Absorbance of LPS-stimulated BV2 cells + vehicle (no test compound)

A_{sample} = Absorbance of LPS-stimulated cells + test compound

ELISA Assay

The concentrations of TNF-α and IL-6 released by activated BV2 microglia following treatment with selected compounds were quantified using commercial ELISA kits (BioLegend, San Diego, CA). The assay was performed according to the manufacturer's protocol. Briefly, collected culture supernatants were transferred to capture antibody-coated 96-well plates and sequentially incubated with detection antibodies, avidin−HRP conjugate, and substrate for colorimetric development. Optical density was recorded at 450 nm, and cytokine concentrations were determined using standard curves.[52,53]

Western Blot Analysis

Total cellular proteins were extracted using radioimmunoprecipitation assay (RIPA) buffer supplemented with protease inhibitors (Thermo Fisher Scientific, Waltham, Massachusetts). Protein concentrations were determined by bicinchoninic acid (BCA) assay (Thermo Fisher Scientific, catalog no. 23227). According to the BCA Protein Assay Kit protocol, protein concentrations were calculated from a BSA standard curve (25−2000 μg/mL) generated for each assay using linear regression analysis. Equivalent amounts of protein (25 μg per lane) were separated by SDS-PAGE and electrotransferred onto polyvinylidene difluoride (PVDF) membranes (Bio-Rad, Hercules, California). Membranes were blocked and incubated overnight at 4 °C with primary antibodies against TNFα (Santa Cruz Biotechnology, Dallas, Texas; sc-52746), NF-κB p65 (Cell Signaling Technology, Danvers, Massachusetts; cst#8242), p-NF-κB p65 (Ser536; cst#3033), and GAPDH (cst#5174). Following incubation with horseradish peroxidase-conjugated secondary antibodies (antirabbit: sc-2357; antimouse: sc-516102), protein bands were visualized using SignalFire enhanced chemiluminescence reagent (Cell Signaling Technology) and quantified with ImageJ software. Target protein expression levels were normalized to glyceraldehyde-3-phosphate dehydrogenase (GAPDH), and relative changes were calculated.[54]

Statistical Analysis

Data were analyzed using GraphPad Prism (San Diego, CA). Results are presented as mean ± SD (at least $n = 3$). Statistical comparisons among groups were performed by one-way ANOVA with Dunnett's and Tukey's post hoc tests. Differences with $p < 0.05$ were considered significant.

■ ASSOCIATED CONTENT

Supporting Information

The Supporting Information is available free of charge at https://pubs.acs.org/doi/10.1021/acsomega.6c01737.

HR-ESI-MS spectra; UV spectra; FT-IR spectra; CD spectra; 1D/2D NMR of compounds **1**−**21**; original Western blot images (Figures S1−S72) (PDF)

■ AUTHOR INFORMATION

Corresponding Author

Boonchoo Sritularak − *Department of Pharmacognosy and Pharmaceutical Botany, Faculty of Pharmaceutical Sciences, Chulalongkorn University, Bangkok 10330, Thailand; Center of Excellence in Natural Products for Ageing and Chronic Diseases, Faculty of Pharmaceutical Sciences, Chulalongkorn University, Bangkok 10330, Thailand;* orcid.org/0000-0001-8352-4122; Email: boonchoo.sr@chula.ac.th

Authors

May Thazin Thant − *Department of Pharmacognosy and Pharmaceutical Botany, Faculty of Pharmaceutical Sciences, Chulalongkorn University, Bangkok 10330, Thailand*

Virunh Kongkatitham − *Department of Pharmacognosy and Pharmaceutical Botany, Faculty of Pharmaceutical Sciences, Chulalongkorn University, Bangkok 10330, Thailand; Center of Excellence in Natural Products for Ageing and Chronic Diseases, Faculty of Pharmaceutical Sciences, Chulalongkorn University, Bangkok 10330, Thailand*

Hnin Ei Ei Khine − *Department of Pharmacology, Faculty of Pharmacy, Mahidol University, Bangkok 10400, Thailand*

Warisara Parichatikanond − *Department of Pharmacology, Faculty of Pharmacy, Mahidol University, Bangkok 10400, Thailand;* orcid.org/0000-0001-7851-2477

Sanith Sri Jayashan − *Department of Pharmacognosy and Pharmaceutical Botany, Faculty of Pharmaceutical Sciences, Chulalongkorn University, Bangkok 10330, Thailand*

Preeyaporn Poldorn − *Synfuels China Technology Co. Ltd., Beijing 101407, China*

Yutthana Wongnongwa − *NSTDA Supercomputer Center (ThaiSC), National Electronics and Computer Technology Center (NECTEC), National Science and Technology Development Agency (NSTDA), Khlong Luang, Pathum Thani 12120, Thailand*

Pasarapa Towiwat − *Department of Pharmacology and Physiology, Faculty of Pharmaceutical Sciences and Animal Models of Chronic Inflammation-Associated Diseases for Drug Discovery Research Unit, Chulalongkorn University, Bangkok 10330, Thailand;* orcid.org/0000-0001-9394-4622

Chotima Böttcher − *Experimental and Clinical Research Center, A Cooperation between the Max Delbrück Center for Molecular Medicine in the Helmholtz Association and Charité-Universitätsmedizin Berlin, Berlin 13125, Germany*

Complete contact information is available at: https://pubs.acs.org/10.1021/acsomega.6c01737

https://doi.org/10.1021/acsomega.6c01737
ACS Omega XXXX, XXX, XXX−XXX

Funding

This research is funded by Thailand Science research and Innovation Fund Chulalongkorn University (HEA_FF_69_061_3300_009).

Notes

The authors declare no competing financial interest.

■ ACKNOWLEDGMENTS

M.T.T. sincerely thanks Chulalongkorn University for awarding a C2F (Second Century Fund) postdoctoral fellowship, conducted under B.S.'s supervision. P.P. gratefully acknowledge support from the SynCat@Beijing, Synfuels China Technology Co. Ltd. Y.W. thanks the NSTDA Supercomputer Center (ThaiSC) for providing computing resources. The authors thank Ms. Wanwimon Mekboonsonglarp for NMR (600 MHz) measurement and Mr. Yanyong Punpreuk for the plant identification. We would like to acknowledge the Pharmaceutical Science Research Instrument Center, Faculty of Pharmaceutical Sciences, Chulalongkorn University for Instrument measurement. We gratefully thank Dr. Chattarika Pengdee for her support in some parts of structural interpretation. We sincerely appreciate Ms. Monsin Sangsawat for her technical contribution to the HPLC-based purity analysis.

■ REFERENCES

(1) Chen, W. W.; Zhang, X. I. A.; Huang, W. J. Role of neuroinflammation in neurodegenerative diseases. *Mol. Med. Rep.* **2016**, *13* (4), 3391−3396.
(2) Shao, F.; Wang, X.; Wu, H.; Wu, Q.; Zhang, J. Microglia and neuroinflammation: crucial pathological mechanisms in traumatic brain injury-induced neurodegeneration. *Front. Aging Neurosci.* **2022**, *14*, No. 825086.
(3) Smith, J. A.; Das, A.; Ray, S. K.; Banik, N. L. Role of pro-inflammatory cytokines released from microglia in neurodegenerative diseases. *Brain Res. Bull.* **2012**, *87* (1), 10−20.
(4) Wang, W. Y.; Tan, M. S.; Yu, J. T.; Tan, L. Role of pro-inflammatory cytokines released from microglia in Alzheimer's disease *Ann. Transl. Med.* 2015; Vol. *3* 1136.
(5) Mamun, A. A.; Shao, C.; Geng, P.; Wang, S.; Xiao, J. Polyphenols targeting NF-κB pathway in neurological disorders: what we know so far? *Int. J. Biol. Sci.* **2024**, *20* (4), No. 1332.
(6) Aryal, B.; Raut, B. K.; Bhattarai, S.; Bhandari, S.; Tandan, P.; Gyawali, K.; Sharma, K.; Ranabhat, D.; Thapa, R.; Aryal, D.; Ojha, A.; et al. Potential therapeutic applications of plant-derived alkaloids against inflammatory and neurodegenerative diseases. *Evidence Based Complement Alternat Med.* **2022**, *2022*, No. 7299778.
(7) Uppala, P. K.; Gudhanti, S. N. K. R.; Alavala, R. R.; Prasanth, D.; Vangoori, Y.Antioxidant and hepatoprotective activity of *Aerides odorata* Lour. on alcohol induced liver damage in rats *Indian J. Pharm. Sci.* 2022; Vol. *84* 5 DOI: 10.36468/pharmaceutical-sciences.
(8) Tokaew, W.; Krubkratoke, D.; Payakdet, S.; Phromprasit, P. Comparative anatomical characters of the genus *Aerides* Lour. (Orchidaceae) in Thailand. *Biodivers. J.* **2023**, *24* (12), 6641−6651, DOI: 10.13057/biodiv/d241226.
(9) Katta, J.; Rampilla, V.; Khasim, S. M. A Study on phytochemical and anticancer activities of epiphytic orchid *Aerides odorata* Lindl. *Eur. J. Med. Plants.* **2019**, *28* (3), 1−21.
(10) Pant, B. Medicinal orchids, and their uses: Tissue culture a potential alternative for conservation. *Afr. J. Plant Sci.* **2013**, *7*, 448−467.
(11) Akter, M.; Huda, M. K.; Hoque, M. M. Investigation of secondary metabolites of nine medicinally important orchids of Bangladesh. *J. Pharmacogn. Phytochem.* **2018**, *7*, 602−606.
(12) Thant, M. T.; Bhummaphan, N.; Wuttiin, J.; Puttipanyalears, C.; Chaichompoo, W.; Rojsitthisak, P.; Punpreuk, Y.; Böttcher, C.; Likhitwitayawuid, K.; Sritularak, B. New phenolic glycosides from *Coelogyne fuscescens* Lindl. var. *brunnea* and their cytotoxicity against human breast cancer cells. *ACS Omega* **2024**, *9* (7), 7679−7691.
(13) Thant, M. T.; Hasriadi, H.; Poldorn, P.; Jungsuttiwong, S.; Rojsitthisak, P.; Böttcher, C.; Towiwat, P.; Sritularak, B. New phenanthrenequinones from *Cymbidium ensifolium* roots and their anti-inflammatory activity on lipopolysaccharide activated BV2 microglial cells. *RSC Adv.* **2024**, *14* (39), 28390−28400.
(14) Majumder, P. L.; Pal, S. Rotundatin, a new 9, 10-dihydrophenanthrene derivative from *Dendrobium rotundatum*. *Phytochemistry* **1992**, *31* (9), 3225−3228.
(15) Chen, Y.; Xu, J.; Yu, H.; Qing, C.; Zhang, Y.; Wang, L.; Liu, Y.; Wang, J. Cytotoxic phenolics from *Bulbophyllum odoratissimum*. *Food Chem.* **2008**, *107* (1), 169−173.
(16) Leong, Y. W.; Kang, C. C.; Harrison, L. J.; Powell, A. D. Phenanthrenes, dihydrophenanthrenes and bibenzyls from the orchid *Bulbophyllum vaginatum*. *Phytochemistry* **1997**, *44* (1), 157−165.
(17) Ono, M.; Ito, Y.; Masuoka, C.; Koga, H.; Nohara, T. Antioxidative constituents from *Dendrobii Herba* (stems of Dendrobium spp.). *Food Sci. Technol. Int.* **1995**, *1* (2), 115−120.
(18) Simmler, C.; Antheaume, C.; Lobstein, A. Antioxidant biomarkers from *Vanda coerulea* stems reduce irradiated HaCaT PGE-2 production as a result of COX-2 inhibition. *PLoS One* **2010**, *5* (10), No. e13713.
(19) Rueda, D. C.; Schöffmann, A.; De Mieri, M.; Raith, M.; Jähne, E. A.; Hering, S.; Hamburger, M. Identification of dihydrostilbenes in *Pholidota chinensis* as a new scaffold for GABAA receptor modulators. *Bioorg. Med. Chem.* **2014**, *22* (4), 1276−1284.
(20) Zhang, X.; Gao, H.; Wang, N.; Yao, X. Phenolic components from *Dendrobium nobile*. *Chin. Tradit. Herb. Drug.* **2006**, 652−655.
(21) González-Baró, A. C.; Parajón-Costa, B. S.; Franca, C. A.; Pis-Diez, R. Theoretical and spectroscopic study of vanillic acid. *J. Mol. Struct.* **2008**, *889* (1−3), 204−210.
(22) Lee, J. M.; Lee, D. G.; Lee, K. H.; Cho, S. H.; Nam, K. W.; Lee, S. Isolation, and identification of phytochemical constituents from the fruits of *Acanthopanax senticosus*. *Afr. J. Pharm. Pharmacol.* **2013**, *7* (6), 294−301.
(23) Majumder, P. L.; Banerjee, S.; Lahiri, S.; Mukhoti, N.; Sen, S. Dimeric phenathrenes from two *Agrostophyllum* species. *Phytochemistry* **1998**, *47* (5), 855−860.
(24) Rivai, B.; Wasana, P. W. D.; Chansriniyom, C.; Towiwat, P.; Punpreuk, Y.; Likhitwitayawuid, K.; Rojsitthisak, P.; Sritularak, B. Potential role of a novel biphenanthrene derivative isolated from *Aerides falcata* in central nervous system diseases. *RSC Adv.* **2023**, *13* (16), 10757−10767.
(25) Zhang, Y.; Yan, G.; Sun, C.; Li, H.; Fu, Y.; Xu, W. Apoptosis effects of dihydrokaempferol isolated from *Bauhinia championii* on synoviocytes. *J. Evidence-Based Complementary Altern. Med.* **2018**, *2018*, No. 9806160.
(26) Klongkumnuankarn, P.; Busaranon, K.; Chanvorachote, P.; Sritularak, B.; Jongbunprasert, V.; Likhitwitayawuid, K. Cytotoxic and antimigratory activities of phenolic compounds from *Dendrobium brymerianum*. *J. Evidence-Based Complementary Altern. Med.* **2015**, *1*, No. 350410.
(27) Majumder, P. L.; Bandyopadhyay, S.; Pal, S. Rigidanthrin, a new dimeric phenanthrene derivative of the orchid *Bulbophyllum rigidum*. *Journal of the Indian Chemical Society* **2008**, *85* (11), 1116−1123.
(28) Thant, M. T.; Sritularak, B.; Chatsumpun, N.; Mekboonsonglarp, W.; Punpreuk, Y.; Likhitwitayawuid, K. Three novel biphenanthrene derivatives and a new phenylpropanoid ester from *Aerides multiflora* and their α-glucosidase inhibitory activity. *Plants* **2021**, *10* (2), No. 385.
(29) Park, H. B.; Lee, K. H.; Kim, K. H.; Lee, I. K.; Noh, H. J.; Choi, S. U.; Lee, K. R. Lignans from the roots of *Berberis amurensis*. *Nat. Prod. Sci.* **2009**, *15* (1), 17−21.

https://doi.org/10.1021/acsomega.6c01737
ACS Omega XXXX, XXX, XXX−XXX

(30) Leong, Y. W.; Harrison, L. J.; Powell, A. D. Phenanthrene and other aromatic constituents of *Bulbophyllum vaginatum*. *Phytochemistry* **1999**, *50* (7), 1237−1241.
(31) Kim, G. J.; Park, S.; Kim, E.; Kwon, H.; Park, H. J.; Nam, J. W.; Roh, S. S.; Choi, H. Antioxidant, pancreatic lipase inhibitory, and tyrosinase inhibitory activities of extracts of the invasive plant *Spartina anglica* (Cordgrass). *Antioxidants* **2021**, *10* (2), No. 242.
(32) Ito, M.; Matsuzaki, K.; Wang, J.; Daikonya, A.; Wang, N. L.; Yao, X. S.; Kitanaka, S. New phenanthrenes and stilbenes from *Dendrobium loddigesii*. *Chem. Pharm. Bull.* **2010**, *58* (5), 628−633.
(33) Lin, C. W.; Hwang, T. L.; Chen, F. A.; Huang, C. H.; Hung, H. Y.; Wu, T. S. Chemical constituents of the rhizomes of *Bletilla formosana* and their potential anti-inflammatory activity. *J. Nat. Prod.* **2016**, *79* (8), 1911−1921.
(34) Hu, J.; Fan, W.; Dong, F.; Miao, Z.; Zhou, J. Chemical components of *Dendrobium chrysotoxum*. *Chin. J. Chem.* **2012**, *30* (6), 1327−1330.
(35) Korver, O.; Wilkins, C. K. Circular dichroism spectra of flavanols. *Tetrahedron* **1971**, *27* (22), 5459−5465.
(36) Pengdee, C.; Dehlinger, A.; Thant, M. T.; Naini, A. A.; Fajriah, S.; Punpreuk, Y.; Mekboonsonglarp, W.; Kongkatitham, V.; Jungsuttiwong, S.; Chaotham, C.; Böttcher, C.; Sritularak, B. Immunomodulatory activity of isolated phenanthrene and dihydrophenanthrene derivatives (coelotrinins A-L) from *Coelogyne trinervis*. *Phytochemistry* **2026**, *241*, No. 114676.
(37) Auberon, F.; Olatunji, O. J.; Herbette, G.; Raminoson, D.; Antheaume, C.; Soengas, B.; Bonté, F.; Lobstein, A. Chemical constituents from the aerial parts of *Cyrtopodium paniculatum*. *Molecules* **2016**, *21* (10), No. 1418.
(38) Alshaye, N. A.; Mughal, E. U.; Elkaeed, E. B.; Ashraf, Z.; Kehili, S.; Nazir, Y.; Naeem, N.; Abdul Majeed, N.; Sadiq, A. Synthesis, and biological evaluation of substituted aurone derivatives as potential tyrosinase inhibitors: *in vitro*, kinetic, QSAR, docking and drug-likeness studies. *J. Biomol. Struct. Dyn.* **2023**, *41* (17), 8307−8322.
(39) Yoshikawa, K.; Eiko, K.; Mimura, N.; Kondo, Y.; Arihara, S. Hovetrichosides C−G, five new glycosides of two auronols, two neolignans, and a phenylpropanoid from the bark of *Hovenia trichocarea*. *J. Nat. Prod.* **1998**, *61* (6), 786−790.
(40) Li, X. C.; Cai, L.; Wu, C. D. Antimicrobial compounds from *Ceanothus americanus* against oral pathogens. *Phytochemistry* **1997**, *46* (1), 97−102.
(41) Elmaidomy, A. H.; Mohyeldin, M. M.; Ibrahim, M. M.; Hassan, H. M.; Amin, E.; Rateb, M. E.; Hetta, M. H.; El Sayed, K. A. Acylated iridoids and rhamnopyranoses from *Premna odorata* (lamiaceae) as novel mesenchymal−epithelial transition factor receptor inhibitors for the control of breast cancer. *Phytother. Res.* **2017**, *31* (10), 1546−1556.
(42) Calabrese, V.; Mancuso, C.; Calvani, M.; Rizzarelli, E.; Butterfield, D. A.; Stella, A. M. G. Nitric oxide in the central nervous system: neuroprotection versus neurotoxicity. *Nat. Rev. Neurosci.* **2007**, *8* (10), 766−775.
(43) Tarafdar, A.; Pula, G. The role of NADPH oxidases and oxidative stress in neurodegenerative disorders. *Int. J. Mol. Sci.* **2018**, *19* (12), No. 3824.
(44) Sui, G.; Li, T.; Zhang, B.; Wang, R.; Hao, H.; Zhou, W. Recent advances on synthesis and biological activities of aurones. *Bioorg. Med. Chem.* **2021**, *29*, No. 115895.
(45) Won, J. H.; Kim, J. Y.; Yun, K. J.; Lee, J. H.; Back, N. I.; Chung, H. G.; Chung, S. A.; Jeong, T. S.; Choi, M. S.; Lee, K. T. Gigantol isolated from the whole plants of *Cymbidium goeringii* inhibits the LPS-induced iNOS and COX-2 expression via NF-κB inactivation in RAW 264.7 macrophages cells. *Planta med.* **2006**, *72* (13), 1181−1187.
(46) Zhou, D.; Chen, G.; Ma, Y. P.; Wang, C. G.; Lin, B.; Yang, Y. Q.; Li, W.; Koike, K.; Hou, Y.; Li, N. Isolation, structural elucidation, optical resolution, and antineuroinflammatory activity of phenanthrene and 9, 10-dihydrophenanthrene derivatives from *Bletilla striata*. *J. Nat. Prod.* **2019**, *82* (8), 2238−2245.
(47) Cheng, W.; Lu, J.; Wang, B.; Sun, L.; Zhu, B.; Zhou, F.; Ding, Z. Inhibition of inflammation-induced injury and cell migration by coelonin and militarine in PM2. 5-exposed human lung alveolar epithelial A549 cells. *Eur. J. Pharmacol.* **2021**, *896*, No. 173931.
(48) Poonasri, M.; Mankhong, S.; Chiranthanut, N.; Srisook, K. 4-methoxycinnamyl *p*-coumarate reduces neuroinflammation by blocking NF-κB, MAPK, and Akt/GSK-3β pathways and enhancing Nrf2/HO-1 signaling cascade in microglial cells. *Biomed. Pharmacother.* **2023**, *168*, No. 115808.
(49) Frisch, M. J.; Trucks, G. W.; Schlegel, H. B.; Scuseria, G. E.; Robb, M. A.; Cheeseman, J. R.; Scalmani, G.; Barone, V.; Mennucci, B.; Petersson, G.; Nakatsuji, H. Uranyl extraction by N, N-dialkylamide ligands studied by static and dynamic DFT simulations. *Dalton Trans.* **2009**, *9* (9), 2623−2638.
(50) Bruhn, T.; Schaumlöffel, A. N. U.; Hemberger, Y.; Bringmann, G. SpecDis: Quantifying the comparison of calculated and experimental electronic circular dichroism spectra. *Chirality* **2013**, *25* (4), 243−249.
(51) Jin, H. G.; Kim, K. W.; Li, J.; Lee, D. Y.; Yoon, D.; Jeong, J. T.; Kim, G. S.; Oh, H.; An, R. B.; Kim, Y. C. Anti-inflammatory components isolated from *Atractylodes macrocephala* in LPS-induced RAW264. 7 macrophages and BV2 microglial cells. *Appl. Biol. Chem.* **2022**, *65* (1), No. 11.
(52) Tabatabaei, M. S.; Ahmed, M. Enzyme-Linked Immunosorbent Assay (ELISA). *Methods Mol. Biol.* **2022**, *2508*, 115−134.
(53) Yoon, C. S.; Lee, H.; Liu, Z.; Lee, H. K.; Lee, D. S. Effects of compounds isolated from *Lindera erythrocarpa* on anti-inflammatory and anti-neuroinflammatory action in BV2 microglia and RAW264.7 macrophage. *Int. J. Mol. Sci.* **2022**, *23* (13), No. 7122.
(54) Khine, H. E. E.; Mangmool, S.; Parichatikanond, W. Exendin-4 improves mitochondrial integrity against cisplatin-induced cardiac damage: Targeting p53 and NF-κB pathways. *Eur. J. Pharmacol.* **2025**, *1007*, No. 178233.

https://doi.org/10.1021/acsomega.6c01737
ACS Omega XXXX, XXX, XXX−XXX